Catalysis Today 157 (2010) 425–431

Contents lists available at ScienceDirect

Catalysis Today

journal homepage: www.elsevier.com/locate/cattod

Transition metal-exchanged LTA zeolites as novel catalysts for methane combustion

Esther Asedegbega-Nieto, Eva Díaz, Aurelio Vega, Salvador Ordóñez*

Department of Chemical Engineering and Environmental Technology, University of Oviedo, Faculty of Chemistry, Julián Clavería s/n, 33006 Oviedo, Spain

ARTICLE INFO

Article history:
Available online 18 June 2010

Keywords:
A-zeolites
Methane oxidation
XPS-speciation
Iron catalysts
Cobalt catalysts
Manganese catalysts
Metal oxides

ABSTRACT

The performance of different transition metal-exchanged zeolites for catalytic combustion of lean methane–air mixtures was studied in this work. Transition metals (Fe, Co, Mn) were incorporated to the parent LTA zeolite by ion exchange, using metal nitrates as precursors. Catalytic performance of these materials was compared to the corresponding to the bulk metal oxides in terms of activity and stability. In general terms, Co-exchanged zeolites present very similar behavior to the parent metal oxide, whereas the Mn-exchanged present very poor performance, and the Fe-exchanged zeolite present markedly better performance than the parent bulk oxide. Characterization of the fresh and used catalysts suggests that the superior behavior of the iron-exchanged zeolite is caused by a change in the reducibility properties of the metal species caused by the interaction with the zeolite framework (observed in TPR and O_2-TPD experiments).

1. Introduction

Deep catalytic combustion of lean methane–air mixtures is currently a key issue in catalyst technology because of the increasing concern about greenhouse effect of these emissions (25 times higher than the corresponding to carbon dioxide). It has been estimated that one third of the total CH_4 was derived from point sources, such as mine emissions, coke ovens, livestock management, wastewater treatment plants, etc. Many of these emissions can be channelled and treated. On the other hand, methane is often chosen as a combustion model compound because it is more difficult to oxidize than most of the other hydrocarbons. For example, we have studied the application of catalytic combustion to the treatment of gaseous emissions from coke ovens, determining that a complete oxidation of methane in these emissions leads to a total abatement of all the other organic pollutants [1].

Concerning to the catalyst development, two groups of catalysts systems are normally used: supported noble metals (Pt, Pd and Rh) [2], and transition metal oxides or mixed metal oxides as bulk or supported catalysts [3]. The first group provides higher conversions at a given temperature, but present poor resistance to thermal deactivation and poisoning, whereas the second one is less active but more thermally stable and cheaper. The choice of the most appropriate support is a critical issue, since the nature and distribution of the active species are strongly dependent on the support and preparation method employed. Alumina, zirconia, and silica are some of the main supports used for combustion catalysts [4], although several works propose the use of zeolite as alternative supports. Zeolites have diverse properties making them valuable as catalysts, catalyst supports, adsorbents and ion exchange materials in a wide variety of industrial processes. The presence of exchanged metal ions in the zeolite matrix as isolated species can prevent metal agglomeration and sintering of catalysts. In addition, the zeolite acid sites also can play a role in the catalyst performance [5].

At this point, H-ZSM-5 is one of the most frequently chosen zeolite for the methane catalytic combustion and it has shown excellent performance when Pd has been used as active phase [6,7]. In most of these studies, high Si/Al ratio zeolites were used, as it is generally accepted that zeolite thermal stability increases as Si/Al ratio increases [8]. However, lower Si/Al ratios lead to increasing amount of exchange sites, which can lead to both more dispersed catalysts, and important modification of the active phase properties because of the interaction of the active phase with the weaker but more disperse zeolite active sites [9]. However, to the best of our knowledge, very few works on zeolites with low Si/Al ratio have been published. In this present work we employ a molecular sieve 5A with a Si/Al ratio of 1. Theoretically, A-zeolite should be a good material for loading active metal species in its framework for methane emissions abatement, because it has higher cation exchange capacity (4 mequiv./g) than other zeolites (2–3 mequiv./g) [10]. At this point, preliminary experiments showed that metal-exchanged A-zeolites show very good performance for aromatics combustion [11]. On the other hand, previous studies have proved that cobalt, manganese and iron oxides are

* Corresponding author. Tel.: +34 985 103 437; fax: +34 985 103 434.
E-mail address: sordonez@uniovi.es (S. Ordóñez).

0920-5861/$ – see front matter © 2010 Elsevier B.V. All rights reserved.
doi:10.1016/j.cattod.2010.05.032

active for this reaction [12–14]. So, these metals were introduced in the zeolite framework with the aim of studying the effect of stabilizing these oxides in 5A zeolite, as well as their effect on methane combustion.

2. Experimental procedure

2.1. Catalysts preparation

Different ion-exchanged zeolites (using Fe, Mn and Co precursors) in their oxidized state, as well as bulk transition metal oxides (using the same elements) were tested as catalysts for methane oxidation. Zeolite-based catalysts were prepared using the calcium-exchanged molecular sieve 5A. Iron, cobalt and manganese were introduced in the zeolite structure by ion exchange, selecting identical conditions of exchangeable cation concentration, temperature and contact time. Aqueous solutions (0.25 mol L^{-1}) of the corresponding nitrate precursors ($Fe(NO_3)_3{\cdot}9H_2O$, $Mn(NO_3)_2{\cdot}4H_2O$ and $Co(NO_3)_2{\cdot}6H_2O$) were mixed with 3 g of the parent zeolite and placed in a water bath at 343 K for 24 h. The resulting exchanged zeolites were filtered until neutral pH to remove the excess unreacted salts, dried over night and thereafter treated in air at 773 K for 4 h.

Bulk metal oxides were prepared from the same transition metal solutions [$Fe(NO_3)_3{\cdot}9H_2O$, $Mn(NO_3)_2{\cdot}4H_2O$ and $Co(NO_3)_2{\cdot}6H_2O$], but without the addition of the Ca-A zeolite. An aqueous NaOH solution (0.1 mol L^{-1}) was added until pH = 8, starting the hydroxide precipitation. This precipitate was filtered and washed until neutral pH, dried and calcined following the same procedure as for the exchanged catalysts. XRD diffraction patterns show that the prepared oxides are crystalline bixbyte (α-Mn_2O_3), hematite (Fe_2O_3), and cobalt spinel (Co_3O_4).

2.2. Reaction studies

Reaction studies were performed at atmospheric pressure in a fixed bed reactor. This reactor consisted of a stainless steel tube of 60 cm length and 9 mm internal diameter. The catalyst (0.5 g), with particle size from 250 to 355 μm, was held in the middle by a stainless steel mesh. The upper and lower parts of the reactor were filled with glass spheres of 1 mm diameter. The catalytic bed was in contact with a thermocouple continuously recording the actual temperature. A gas flow of 0.5 L min^{-1} (s.t.p.) of a mixture of dilute methane (2.5 vol.% CH_4 in air of 50 N nominal purity) and purified air from a compressor (Ingersoll-Rand) was fed. The resulting concentration was of 500 ppm, and the weight hourly space velocity (WHSV) was of 77 h^{-1} (0.75 g h $mmol^{-1}$). Reaction products were analyzed in an Agilent gas chromatograph equipped with two capillary columns (HP-Molsiev and HP-Plot Q) in series and FID and TCD detectors. Thereafter, a 50 h deactivation test was performed at a constant temperature of 873 K. In order to study the catalyst ageing, a second activity test was performed after 50 h on the CH_4/air stream (500 ppm of CH_4) at 873 K.

2.3. Catalysts characterization

Crystallinity of the exchanged zeolites (before and after reaction) was measured by XRD using a Philips PW 1710 diffractometer, working with the Cu K_α line (λ = 0.154 nm) in the range 2θ between 5° and 85° at a scanning rate of 2° in 2θ/min. Morphology of samples were determined by transmission electronic microscopy performed in a JEOL JEM 2000 EXII microscope. Textural characteristics of specific surface area and pore volume were estimated by nitrogen adsorption at 77 K in a Micromeritics ASAP 2020 surface area and porosity analyzer. Temperature-programmed reduction was carried out in a Micromeritics TPD/TPR 2900 apparatus coupled with a mass spectrometer analyzer. Pure CuO standard was used for TPR calibration. These experiments were performed with catalyst samples (10 mg) placed in a U-shaped quartz reactor. A high purity mixture of 10% hydrogen in argon was fed into the reactor. The temperature of the sample was increased from 350 to 1100 K at a rate of 10 K min^{-1}. The same apparatus was used for O_2-TPD. In this case, the sample was firstly cleaned at 673 K, then cooled to 320 K and saturated with O_2 (2% in argon) for 30 min. There after samples were purged for 30 min in He before starting the TPD experiments under He from 325 to 1225 K. The lower density of the metal-exchanged zeolites (if compared to other bulk oxides), as well as the analytical limits of the MS detector, do not allow the quantification of the oxygen releases during the O_2-TPD experiments.

Catalyst surface was analyzed by X-ray photoelectron spectroscopy (XPS) with a SPECS Phoibos MCD5 system equipped with a hemispherical electron analyzer operating in a constant pass energy, using Mg Kα radiation ($h\nu$ = 1253.6 eV). The samples were fixed to the sample holder using a carbon adhesive tape. The background pressure in the analysis chamber was kept below 5×10^{-9} mbar during data acquisition. Survey scan spectra were made at a pass energy of 90 eV, while the Si 2p, Al 2p, Mn $2p_{3/2}$, Co $2p_{3/2}$ and Fe $2p_{3/2}$ individual high resolution spectra were taken at a pass energy of 20 eV. All binding energies (BE) were referenced to the C 1s line at 284.6 eV.

3. Results and discussion

3.1. Reaction studies

The performance of the transition metal-exchanged zeolites and mechanical mixtures of the parent A-zeolite and bulk transition metal oxide (with the same amount of metal in both cases) is depicted in Fig. 1. Results presented correspond to the fresh materials (Fig. 1a) and the materials after 52 h on stream at 873 K in presence of the reactive mixture (Fig. 1b). Normalized results, expressed as mmol of methane converted per second and atom of metal are summarized in Fig. 2, based both the bulk composition of the catalysts (Fig. 2a) and the surface concentration, measured by XPS (Fig. 2b). Regarding the activity of the bulk oxides, it is observed that the activity decreases in the order $Co_3O_4 > MnO_2 > Fe_2O_3$. This is in agreement with literature findings where Co_3O_4 has been considered as the most active metal oxide catalysts [15], the following sequence being reported by Paredes et al.: $Co_3O_4 > Mn_2O_3 > CuO > NiO > Cr_2O_3 > Fe_2O_3$ [13,14]. Therefore, the mechanical addition of zeolite A (negligible conversions were obtained when the reactor is loaded only with the parent zeolite) does not seem to have any noticeable effect on the catalyst performance.

The behavior of the ion-exchanged zeolites is completely different depending on the exchanged metal. So, the performance of the Co-exchanged and Mn-exchanged zeolites is worse than the corresponding to the respective oxides, whereas the performance of the iron-exchanged zeolites is largely better than the corresponding bulk oxide. This result suggests that the interaction of the iron oxide with the zeolite improves its catalytic performance. The specific reactivity of the exchanged zeolites, expressed as mmol of methane converted per second and metal atom (considering the bulk composition of the materials determined by ICP-MS) decreases in the order Fe ≈ Co > Mn. If the surface composition (XPS) is considered (Fig. 2b), the specific activity decreases in the order Fe > Mn > Co.

The obtained results were kinetically analyzed considering pseudo-first order kinetics on methane partial pressure, zero order for oxygen (due to its high concentration), and Arrhenius dependence of the kinetic constant. These power-law dependences were usually found in the literature for methane combustion, being considered to be useful for catalyst comparison as well as for

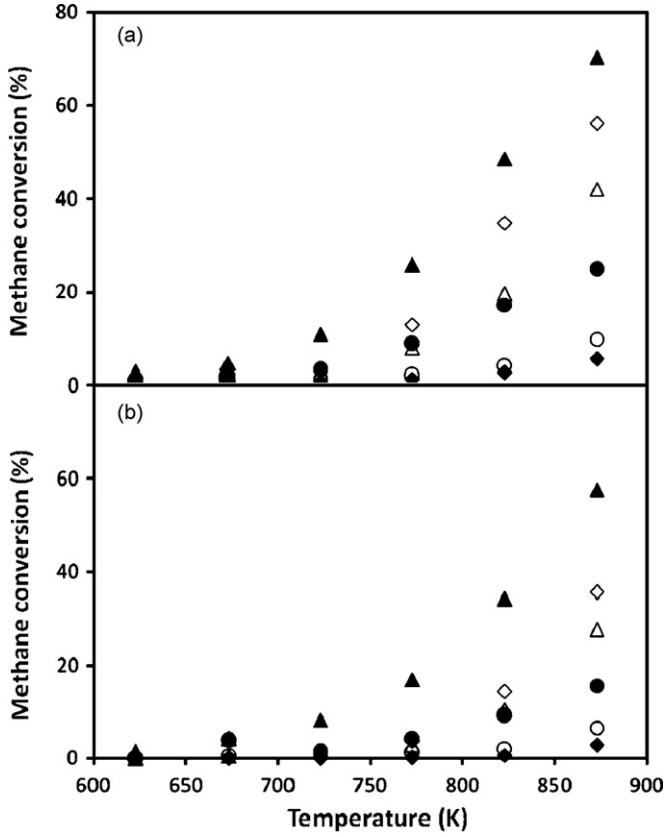

Fig. 1. Evolution of methane conversion with reaction temperature for the fresh (a) and aged (52 h on stream at 873 K; b) studied catalysts: Fe (◊), Co (△), and Mn (○). Closed symbols correspond to bulk oxides and open symbols correspond to metal-exchanged A-zeolite.

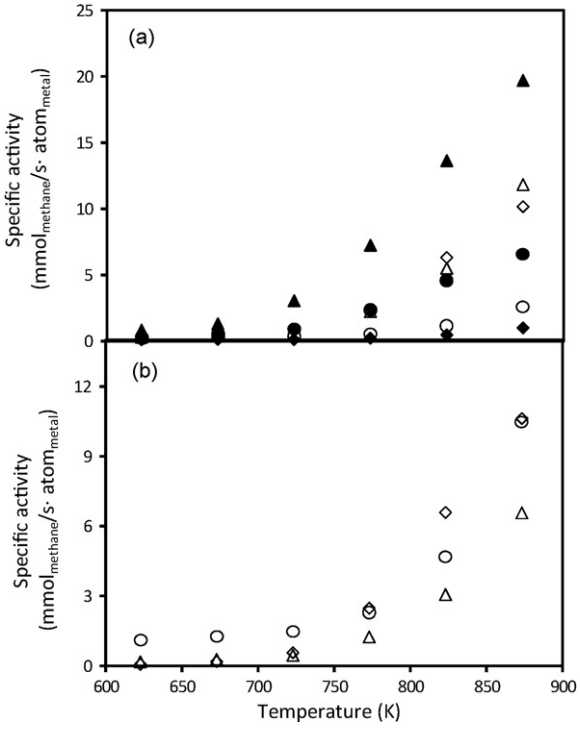

Fig. 2. Specific activity (expressed as mmol of methane converted per second and per metal atom). Results were referred to bulk metal content (a) and to the surface metal content (b). For symbols, see Fig. 1.

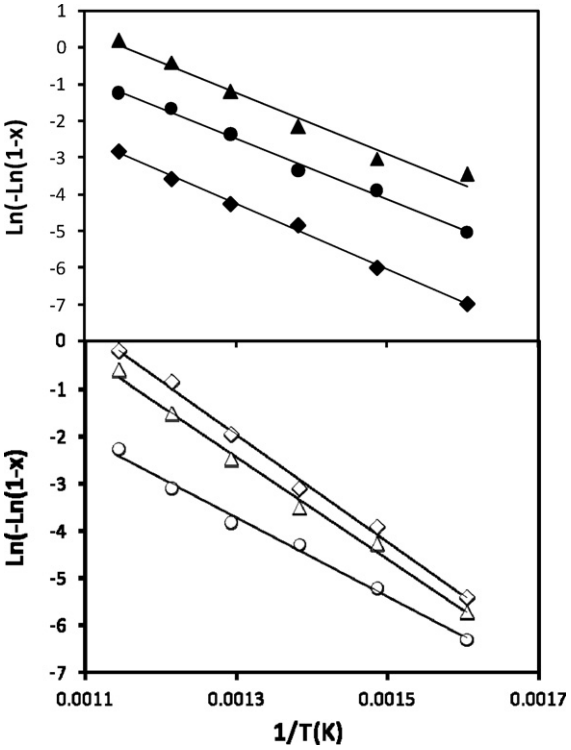

Fig. 3. Pseudo-first order fit (using Eq. (1)) for the experimental data obtained for the combustion of 500 ppm of CH_4 over the bulk oxides (top) and the metal-exchanged zeolites (bottom). For symbols, see Fig. 1.

preliminary reactor design. These assumptions were considered as valid for the catalytic combustion of methane in methane–air diluted mixtures over different catalysts [16]. If plug flow-like behavior for the reactor is supposed, and neglecting the change in density of the reactant gas associated to the reaction (as methane is very diluted), the following equation can be obtained for the integral reactor:

$$\ln(-\ln(1-x)) = \ln(k_0 \cdot p_0 \cdot \tau) - \frac{E_a}{RT} \quad (1)$$

where "ln" means the natural logarithm of the given expression, x is the fractional conversion of methane, τ is the space time, and p_0 is the methane initial partial pressure. Conversions between 1 and 50% were fit to Eq. (1). It can be inferred that these experiments were carried out in the kinetic regime (without external/internal mass and heat transfer limitations), since in previous works, it was both theoretically and experimentally demonstrated for this reaction and this experimental device, working at the same experimental conditions but with a largely more active catalyst (Pd/Al_2O_3 catalyst) that these effects are not affecting the overall reaction kinetics [16].

Pre-exponential factor and activation energy obtained for the six catalysts tested in this work, as well as the regression coefficient for each experiment, are reported in Table 1, whereas the goodness of the numerical fit is observed in Fig. 3. It is observed that in the case of Mn, kinetic parameters for the bulk oxide and for the exchanged zeolite are very similar, whereas in the case of Co and, more markedly, Fe, important differences were observed between both sets of parameters. In both cases, the metal-exchanged zeolites showed higher activation energies and also higher pre-exponential factors, suggesting a different kind of interaction between reactants and active phase.

Concerning the stability of the catalysts, ageing experiments were carried out with the six catalysts at 873 K for 52 h, using 500 ppm of CH_4 in air as reactor feed. Thermal deactivation was

Table 1
Pseudo-first order kinetic parameters and deactivation kinetic constants (considering independent deactivation) for the oxidation of methane over the studied materials.

Catalyst	k_0 (mol kg^{-1} s^{-1} MPa^{-1})	E_a (kJ mol^{-1})	r^2 (kinetics)	k_d (s^{-1})	r^2 (deactivation)
Fe_2O_3	5.78×10^3	69.6	0.989	13.3	0.902
Co_3O_4	1.43×10^5	70.9	0.977	22.5	0.963
Mn_2O_3	2.73×10^4	68.3	0.993	29.0	0.921
Fe-A	5.37×10^6	99.6	0.983	39.6	0.918
Co-A	3.71×10^5	84.3	0.969	27.3	0.987
Mn-A	1.05×10^4	70.2	0.966	1.8	0.905

observed in all the cases. This effect has been modeled according to the Levenspiel procedure [17] considering independent deactivation (deactivation rate showing a first order dependence on catalyst activity) and pseudo-first order kinetics for the main reaction. Catalyst activity was defined as the ration between the reaction rate at a given time and the reaction time extrapolated at $t = 0$. The resulting integrated equation is:

$$\ln(-\ln(1-x)) = \ln(k \cdot \tau) - k_d \cdot \tau \quad (2)$$

where k is the kinetic constant for the main reaction and k_d is the deactivation kinetic constant.

Values of the deactivation constants and the regression coefficient are also summarized in Table 1, showing that the catalysts prepared from A-zeolite are more prone to deactivation than the parent bulk oxides (the case of Mn-exchanged zeolite is not representative because of it is largely less active). Light-off curves recorded after this deactivation experiment (shown in Fig. 1b) entirely confirm this behavior.

3.2. Characterization of fresh and aged catalysts

In order to elucidate the causes of the different behavior of the studied catalysts, fresh and aged catalysts were characterized by different techniques. N_2 adsorption isotherms of fresh and aged catalysts are shown in Fig. 4, whereas the main morphological parameters are reported in Table 2. Parent zeolite shows a type I isotherm characteristic of microporous materials. The introduction of the exchange cation causes a reduction in surface area, this difference being the highest for the iron-exchanged zeolite. This material shows a type IV isotherm, typical of mesoporous materials. This transformation is confirmed by the complete absence of micropores (Table 2). Concerning to the aged samples, it is observed that the porous structure of the parent material is severely affected by the thermal treatment. However, Mn-exchange stabilizes the material, whereas Fe- and Co-exchanged materials present decreases surface areas after reaction (17 and 6%, respectively). Transmission electronic microscopy (TEM) micrographs were also obtained, no significant morphological differences between fresh and aged samples being observed in all the cases. XRD patterns for the fresh exchanged zeolites are depicted in Fig. 5. Crystallinity losses (also shown in Fig. 5) were calculated according to the method proposed in the literature, based on the rate between the intensities of the characteristic diffraction peak and considering 100% for the parent zeolite [15,16]. A loss of the crystallinity has been observed in all the cases, manganese exchanged zeolites retaining the largest degree of crystallinity, whereas Fe-exchanged zeolites completely

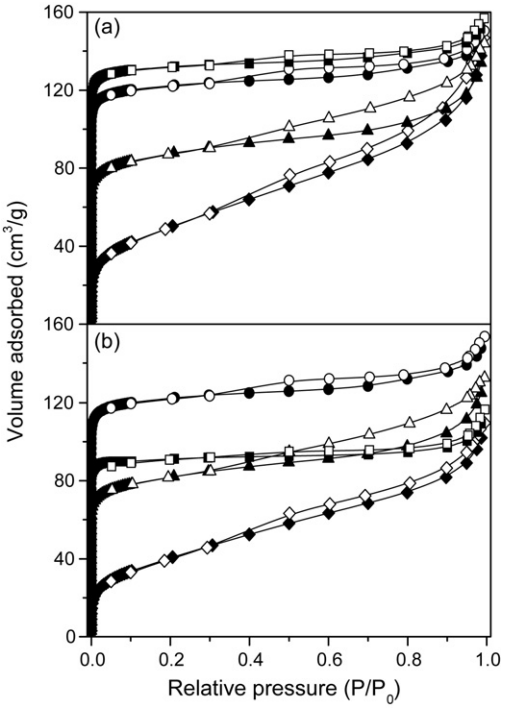

Fig. 4. Nitrogen physisorption isotherms for Fe-(◊), Co-(△), and Mn-(○) exchanged zeolites as well as the parent zeolite (□): fresh (a) and aged (b). Closed and open symbols correspond to adsorption and desorption branches, respectively.

losses its crystalline structure. The chemical analysis of the materials (11.5% for Fe-exchanged zeolites, 7.8% for the Co-exchanged, and 7.7% for the Mn-exchanged-as determined by ICP-MS) is similar to results reported in the literature [11], suggesting that the exchange of aluminium of the zeolites framework by iron ions is the main responsible of these crystallinity losses. Likewise, crystallinity losses of the parent zeolite exposed to the same temperature cycle suggest that thermal effects are the responsible of these crystallinity losses, rather than the reaction itself.

Temperature-programmed reduction profiles of fresh and aged catalysts, as well as that of the corresponding bulk oxide are shown in Fig. 5. The corresponding amounts of H_2 consumption are reported in Table 3. TPR profiles were recorded using the same amount of metal in the bulk oxide and in the metal-exchanged zeolites. The reducibility properties of the exchanged zeolites are completely different depending on the exchanged cation. The iron-

Table 2
Main morphological parameters of the exchanged zeolites before and after the reaction.

Catalyst	Fresh			Aged		
	$S_{Langmuir}$ (m^2 g^{-1})	$V_{mesopores}$ (cm^3 g^{-1})	$V_{micropores}$ (cm^3 g^{-1})	$S_{Langmuir}$ (m^2 g^{-1})	$V_{mesopores}$ (cm^3 g^{-1})	$V_{micropores}$ (cm^3 g^{-1})
Ca-A	573	0.042	0.189	396	0.041	0.131
Mn-A	531	0.048	0.169	531	0.053	0.167
Co-A	382	0.098	0.098	358	0.089	0.091
Fe-A	233	0.178	–	192	0.129	–

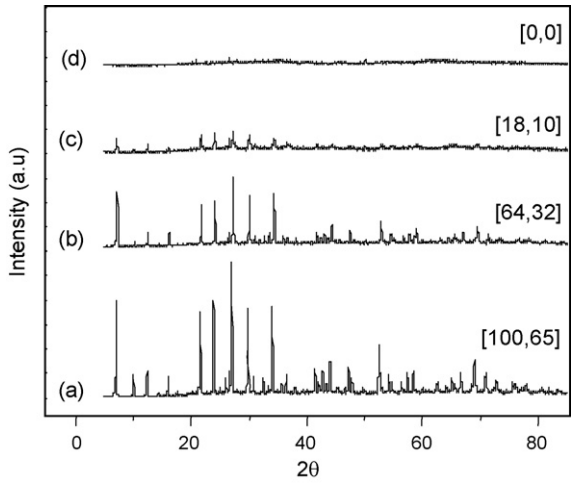

Fig. 5. XRD diffraction patterns for the fresh zeolite-based catalysts used in this work: parent LTA zeolite (a); Mn-exchanged zeolite (b), Co-exchanged zeolite (c), and Fe-exchanged zeolite (d). The relative crystallinity of the fresh (left) and aged (right) materials is summarized in brackets.

exchanged zeolite presents the typical two-step reduction pattern similar to the corresponding to the bulk Fe_2O_3, but displaced to lower temperatures (ca. 100 K) for each peak. The relative proportions of both peaks are also different, being the first peak bigger for the exchanged zeolite. This result suggests that the interaction of the iron ions with the zeolite changes its chemical properties, promoting its reduction. In the case of cobalt, the behavior is just the opposite. In this case, the bulk oxide shows only a reduction peak, which is split into two peaks – with a decreased amount of released hydrogen – and moved to higher temperatures (ca. 350 K in the case of the main reduction peak). In the case of Mn, the reduction temperatures and profiles of the bulk and zeolite-exchanged materials are very similar, a widening of the peaks being the only remarkable effect. Concerning to the hydrogen consumption, similar values were obtained for both kinds of catalysts, suggesting that there are not important differences between the oxidation states of the transition metal species in both cases. In summary, the interaction of the metal ion with the zeolite structure has a positive effect on iron reducibility, negative effect on cobalt reducibility, and no noticeable effects on manganese reducibility. If these results are compared with the reactivity trends discussed before, it should be noted that in the case of the bulk oxides, there is a correlation between the bulk oxide reactivity (Co > Mn > Fe) and the temperature of the reduction peaks (Fe is reduced at the highest temperature). By contrast, in the case of the metal-exchanged zeolites, the reduction temperatures decreases in the order Mn > Co > Fe, which is different to the reactivity order (Fe > Mn > Co, considering the surface concentration). Considering

Table 3
H_2 consumptions ($mol_{H_2}/atom_{metal}$), and temperatures of the maximum of consumption peaks for the TPR of the studied materials.

	Peak 1		Peak 2		Total
	T (K)	H_2/metal	T (K)	H_2/metal	H_2/metal
Fe_2O_3	860	0.27	959	0.93	1.19
Fe-A-fresh	770	0.57	910	0.91	1.48
Fe-A-used	790	0.44	–	–	0.44
Co_3O_4	654	3.96	–	–	3.96
Co-A-fresh	727	1.09	1006	1.07	2.16
Co-A-used	744	0.69	1033	1.00	1.70
Mn_2O_3	656	0.60	728	0.90	1.50
Mn-A-fresh	618	0.53	757	0.85	1.38
Mn-A-used	588	0.44	744	0.67	1.11

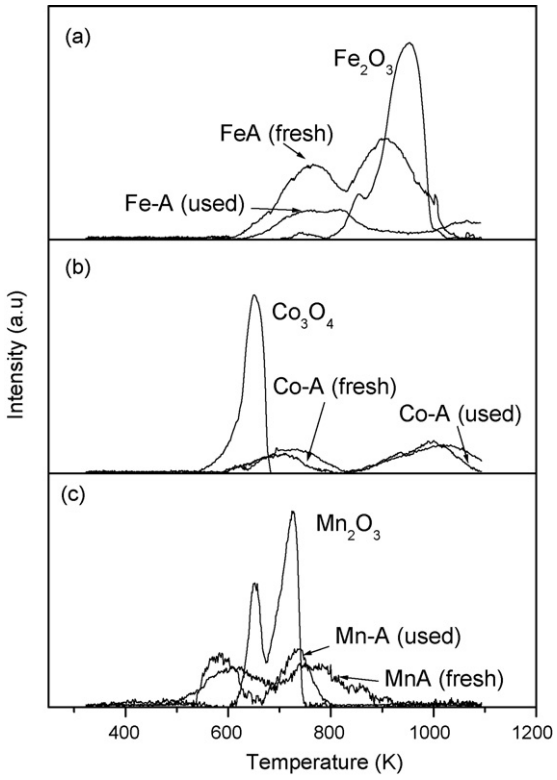

Fig. 6. TPR profiles (H_2 consumption) of the Fe- (a), Co- (b) and Mn- (c) exchanged zeolites, in fresh and used form. TPR profiles of the bulk oxides are also provided.

that methane catalytic combustion over this kind of catalysts is assumed to follow a Mars-van Krevelen mechanism, in which the catalyst is successively reduced by the hydrocarbon and oxidized by the molecular oxygen, increases in the reducibility of the catalysts will lead to higher specific activities. The over-performance of the Fe-exchanged zeolite can be explained considering both that the values of the reduction temperatures are much closer in the zeolites than in the case of the bulk oxides, and the importance of other effects, such as the oxygen mobility in the oxide and the effect of the framework structure.

TPR of the aged catalysts (also shown in Fig. 6) show only minor differences with the corresponding to the fresh catalysts, except in the case of the Fe-exchanged zeolite. In this case, the intensity of high temperature peaks is markedly lower and displaced to higher temperatures. These changes in the reduction properties of the catalyst can justify the observed deactivation.

Temperature-programmed desorption profiles of adsorbed oxygen (O_2-TPD), Fig. 7, also provide valuable information at this point. In the case of bulk oxides, oxygen releases take place at temperature higher than 1000 K, so that are associated to reticular oxygen (also known as β-oxygen [18,19]) rather than to chemisorbed oxygen. In the case of the bulk Fe_2O_3, oxygen releases were not observed in the studied interval, in good agreement with the high thermal stability of this oxide [14]. The amount of released oxygen is in good agreement with the activity trends reported for the bulk oxides: Co oxide is the oxide releasing highest amount of O_2 and is also the most active, whereas Fe_2O_3 release very small amounts of O_2 and is the less active.

When the same experiments are carried out with exchanged zeolites, three different behaviors are observed. In the case of Mn-A, the shape of the O_2 profile is very similar, but the release is displaced to higher temperatures, whereas for the Co-A, the temperature of the maximum release is very similar, but the shape of the desorption peak is markedly wider. In the case of iron-exchanged zeolite,

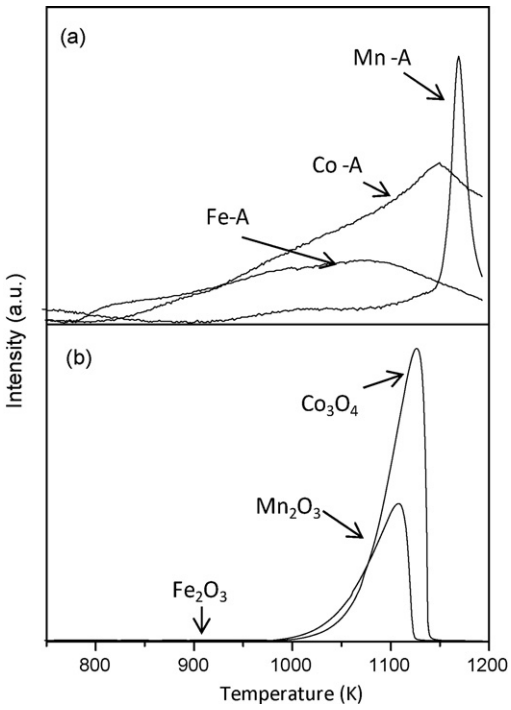

Fig. 7. O_2-TPD profiles (oxygen release) of ion-exchanged zeolites (a), and bulk oxides (b).

a wide desorption peak, not present in the bulk oxide, is observed. Considering that the presence of mobile oxygen species is needed for the catalytic cycle, the presence of this new peak seems to be related with the increase of the activity. Likewise, the availability of oxygen at the work temperatures enhances the catalytic performance, thus the lower the temperature of oxygen release, the more favourable for reaction [11]. As in the case of the TPR results, the interaction of Fe ions with the zeolite largely changes the reactivity of the ion, leading to more active catalytic phase.

In order to gain further understanding on the chemical nature of the metal ions in the exchanged zeolites, XPS analysis of both bulk oxides and transition metal-exchanged zeolites were carried out. Chemical compositions of the exchanged zeolites, fresh and aged, were determined. The first parameter to be considered is the Si/Al ratio (which indicates the changes in the zeolite properties during the exchange), that is close to 1 for both Co-A and Mn-A – not differing so much from the parent zeolite, Ca-A (1.11). In the case of Fe-A, this ratio is four times increased (3.99), indicating that the introduction of iron causes important dealumination effects. That is so because of the chemical similarity between Fe and Al ions [20,21, and references cited therein]. This exchange is the main responsible of the morphological and crystallographic changes previously mentioned. Differences are also observed in the metal surface (XPS results) and bulk (ICP results) concentrations. In the case of the Fe-exchanged zeolite, both values are very similar (11 and 11.5%), indicating that the catalyst is a homogenous solid, without any kind of surface heterogeneity. Concerning to Co-exchanged zeolite, surface concentration is larger than bulk concentration (14% vs. 7.8%), whereas in the case of the Mn-exchanged zeolite, the situation is just the opposite (2% vs. 7.7%). Thus, Mn ions trend to be introduced in the internal zeolite structure – although the zeolite structure is not largely modified – hence, justifying the low activity of the Mn-exchanged zeolite. In the case of the Co ions, they trend to concentrate in the surface of the zeolite. Likewise, from the crystallinity losses of the exchanged zeolite and the variation of Co TPR profiles, it is observed that the interaction of the ion with the zeolite is important. XPS analyses were also carried out with the aged samples. Although no variation in the chemical nature of the metals were observed, a significant decrease of the metal surface concentration was detected for all the metal-exchanged zeolites (about 30% for Co and Mn; and 50%

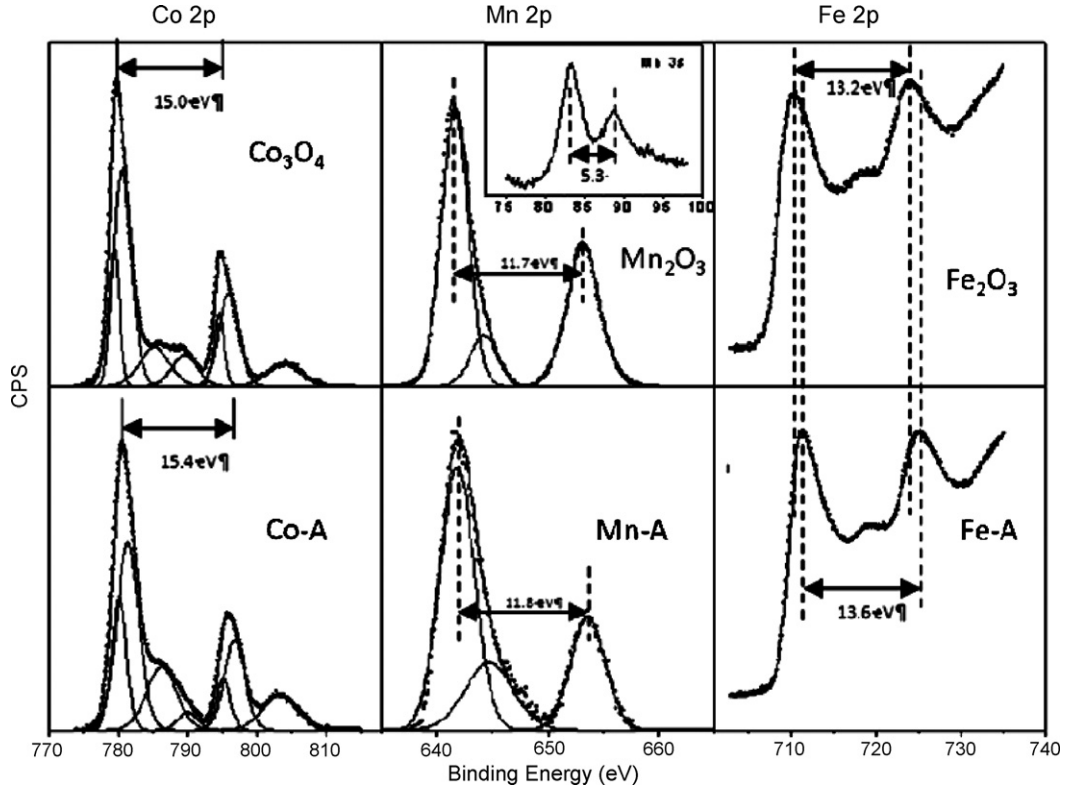

Fig. 8. High resolution XPS spectra for fresh Co, Mn and Fe catalysts. Upper spectra correspond to metal-exchanged zeolite, and downer ones correspond to the bulk oxides.

for Fe). This fact also justifies the faster deactivation observed for the Fe-exchanged zeolites. High resolution spectra of the transition metals on both kinds of catalysts were recorded in order to gain further understanding on the chemical nature of these ions within the zeolite structure. The Co 2p spectra corresponding to the bulk oxide is given in Fig. 8a. Two dissymmetric peaks centred at 779.8 and 794.8 eV due to $2p_{3/2}$ and $2p_{1/2}$, respectively, can be observed. The deconvolution of both peaks gave rise to two components owing to the presence of Co^{2+} and Co^{3+} [22]. These results are in good agreement with literature findings typical for Co_3O_4 [23]. Peaks observed for this oxide were also present in the Co-A exchanged zeolite, although $2p_{3/2}$ and $2p_{1/2}$ binding energies have shifted to higher values, because of the interaction between Co and the zeolite framework. The highest Co $2p_{3/2}$–Co $2p_{1/2}$ separation (15.4 eV vs. 15 eV) is representative of the increase in Co^{2+} [22,23].

In the case of bulk Mn oxide, two peaks at 641.4 and 653.1 eV were observed, corresponding to the $2p_{3/2}$ and $2p_{1/2}$ of Mn_2O_3, respectively [22], whereas the broad peak at around 644.5 eV is due to energy losses. Furthermore, the extent of Mn 3s splitting (5.3 eV) confirms that Mn_2O_3 was the prepared oxide [24]. For the exchanged zeolites (Fig. 7d) slightly higher values (653.6 and 641.7 eV) were observed indicating that the surface Mn species show a very slight interaction with the zeolite framework, in good agreement with the TPR and O_2-TPD measurements.

XPS spectra of the bulk Fe oxide as well as the exchanged zeolite are given in Fig. 8e and f. Main Fe 2p peaks at 710.6 and 723.8 eV correspond to Fe_2O_3 [25,26]. In the case of the iron-exchanged zeolite, a slight shift of the profile to higher binding energies is observed, suggesting a weak interaction with the zeolite structure, not modifying the iron oxidation state. Thus, the chemical state of the iron ion in the zeolite and in the bulk oxide is similar, but the presence of the zeolite structure promotes the redox changes that improve the catalytic performance of the material.

4. Conclusions

Transition metals (Fe, Co and Mn) exchanged LTA zeolites are active for methane combustion, although they show different performance. The most outstanding behavior has been observed for Fe-exchanged zeolite, showing a catalytic activity largely higher than the parent metal oxide. Characterization of the studied catalysts suggests that this behavior is caused by changes in the reducibility of the iron species in the exchanged zeolite (as observed in the shift of the TPR profiles to lower temperatures).

Concerning the stability of the catalysts, zeolite-based catalysts are more prone to deactivation than the parent bulk oxides. Catalyst deactivation can be attributed to a decrease in the surface metal content of the exchanged zeolites, as well as to a change on the reduction properties of the catalysts.

Acknowledgement

E. Asedegbega-Nieto thanks the Spanish Ministry of Education and Science for financing her research within the “Juan de la Cierva” post-doctoral program.

References

[1] P. Hurtado, S. Ordóñez, H. Sastre, F.V. Díez, Appl. Catal. B 47 (2004) 85.
[2] P. Gélin, M. Primet, Appl. Catal. B 39 (2002) 1.
[3] M.F.M. Zwinkels, S.G. Jaras, P.G. Menon, T.A. Griffin, Catal. Rev.: Sci. Eng. 35 (1993) 319.
[4] L.S. Escandón, S. Ordóñez, A. Vega, F.V. Díez, Chemosphere 58 (2005) 9.
[5] L. Intriago, E. Díaz, S. Ordóñez, A. Vega, Microporous Mesoporous Mater. 91 (2006) 161.
[6] S. Arnone, G. Bagnasco, G. Busca, L. Lisi, G. Russo, M. Turco, Stud. Surf. Sci. Catal. 119 (1998) 65.
[7] F. Porcher, M. Souhassou, H. Graafsma, A. Puig-Molina, Y. Dusausoy, C. Lecomte, Acta Cryst. B 56 (2000) 766.
[8] G. Cruciani, J. Phys. Chem. Solids 67 (2006) 1973.
[9] A. Dyer, Stud. Surf. Sci. Catal. 168 (2007) 525.
[10] S. Hui, C.Y.H. Chao, Environ. Sci. Technol. 42 (2008) 7392.
[11] E. Díaz, S. Ordóñez, A. Vega, J. Coca, Appl. Catal. B 56 (2005) 313.
[12] S. Ordóñez, J.R. Paredes, F.V. Diez, Appl. Catal. A 341 (2008) 174.
[13] J.R. Paredes, E. Díaz, F.V. Díez, S. Ordóñez, Energy Fuels 23 (2009) 86.
[14] J.R. Paredes, S. Ordóñez, A. Vega, F.V. Díez, Appl. Catal. B 47 (2004) 37.
[15] J.H. Lee, D.L. Trimm, Fuel Process. Technol. 42 (1995) 339.
[16] P. Hurtado, S. Ordóñez, H. Sastre, F.V. Díez, Appl. Catal. B 51 (2004) 229.
[17] O. Levenspiel, Chemical Reaction Engineering, 3rd ed., Wiley, New York, 1999, p. 473.
[18] M.R. Morales, B.P. Barbero, L.E. Cadús, Appl. Catal. B 74 (2007) 1.
[19] J. Kirchnerova, M. Alifanti, B. Delmon, Appl. Catal. A 231 (2002) 65.
[20] E. Díaz, S. Ordóñez, A. Vega, J. Coca, J. Chromatogr. A 1049 (2004) 161.
[21] R. López-Fonseca, B. De Rivas, J.I. Gutiérrez- Ortiz, A. Aranzabal, J.R. González-Velasco, Appl. Catal. B 41 (2003) 31.
[22] J.M. Giraudon, A. Elhachimi, F. Wyrwalski, S. Siffert, A. Aboukais, J.F. Lanonier, G. Leclerq, Appl. Catal. B 75 (2007) 157.
[23] H.A.E. Hagelin-Weaver, G.B. Hoflund, D.M. Minahan, G.N. Salaita, Appl. Surf. Sci. 235 (2004) 420.
[24] Y.F. Han, L. Chen, K. Ramesh, Z. Zhong, F. Chen, J. Chin, H. Mook, Catal. Today 131 (2008) 35.
[25] T.K. Ghorai, S. Pramanik, P. Pramanik, Appl. Surf. Sci. 255 (2009) 9026.
[26] B.M. Weckhuysen, D. Wang, M.P. Rosynek, J.H. Lunsford, J. Catal. 175 (1998) 347.